

# A Geometric Transversals Approach to Sensor Motion Planning for Tracking Maneuvering Targets

Hongchuan Wei, *Student Member, IEEE*, and Silvia Ferrari, *Senior Member, IEEE*

**Abstract**—This technical note presents a geometric transversals approach for representing the probability of track detection as an analytic function of time and target motion parameters. By this approach, the optimization of the detection probability subject to sensor kinodynamic constraints can be formulated as an optimal control problem. Using the proposed detection probability function, the necessary conditions for optimality can be derived using calculus of variations, and solved numerically using a variational iteration method (VIM). The simulation results show that sensor state and control trajectories obtained by this approach bring about a significant increase in detection probability compared to existing strategies, and require a computation that is significantly reduced compared to direct methods.

**Index Terms**—Detection theory, geometric transversals, mobile sensor networks, optimal control, target tracking, track coverage.

## I. INTRODUCTION

The problem of tracking moving targets by means of a mobile sensor network is relevant to a wide range of applications, including environmental and atmospheric monitoring, security and surveillance, tracking of endangered species, and condition-based diagnostics [1]–[3]. It has been previously shown that the quality-of-service (QoS) of sensor networks performing cooperative target tracking can be quantified by track coverage functions derived using geometric transversals and probability theory, assuming targets move at constant speed and heading in the region-of-interest (RoI) [4], [5].

Recently, the geometric transversals approach in [4] was extended to maneuvering targets described by Markov motion models and used to optimize the detection probability of static sensor networks [6]. This technical note extends the results in [6] to the problem of tracking a maneuvering target by a network of omnidirectional sensors mounted on mobile vehicles, and referred to simply as *mobile sensors*. The advantage of mobile sensors over static sensors is that, over time, they can cover larger portions of the RoI, and they can plan their paths based on where targets are expected to travel to at future times. Although optimal control has been previously applied to mobile sensor networks, its applicability is often limited by the lack of suitable objective functions. This technical note shows that, using the proposed track coverage function, optimal control can be used to obtain optimality conditions and solutions for maximizing the detection probability over time, based on the probability distributions describing the target Markov motion model.

There is considerable precedence in the tracking and estimation literature for modeling target dynamics by Markov motion models [7], [8]. Using the approach presented in this technical note, mobile sensors can be controlled based on the Markov transition probability density functions (pdfs) that are routinely outputted by tracking and estimation algorithms [7], [9]. Because the track coverage function is not quadratic, the optimal control problem may be solved using direct or indirect numerical methods [10], [11]. Direct methods determine near optimal solutions by discretizing the continuous-time problem and transcribing it into a finite-dimensional nonlinear program (NLP). Thus, they may become intractable for more than a few sensors. Using the proposed track coverage function, this technical note derives necessary conditions for optimality, also known as Euler–Lagrange (EL) equations, and then determines a numerical solution using a variational iteration method (VIM) that exploits the integro-differential structure of the EL equations to reduce computational complexity. The numerical simulations show that, by this approach, the detection probability is significantly increased compared to existing potential field, greedy, grid, and random deployment algorithms.

## II. SENSOR NETWORK MOTION PLANNING (SNMP)

### PROBLEM FORMULATION

This technical note considers the problem of planning the state and control trajectories of a network of  $n$  mobile sensors that seek to cooperatively detect a moving target in a two-dimensional RoI,  $\mathcal{A} = [0, L_x] \times [0, L_y]$ , during a fixed time interval  $(T_0, T_f]$ . Each sensor is mounted on a vehicle that is assumed to obey linear and time-invariant (LTI) equations of motion. Let  $\mathbf{s}_i \in \mathcal{A}$  and  $\mathbf{u}_i \in \mathbb{R}^2$  denote the state and control of the  $i$ th vehicle, respectively, such that  $\mathbf{s} = [\mathbf{s}_1^T \dots \mathbf{s}_n^T]^T$  and  $\mathbf{u} = [\mathbf{u}_1^T \dots \mathbf{u}_n^T]^T$  denote the state and control of the sensor network, respectively. Then, the network dynamics can be represented by the state-space equation

$$\dot{\mathbf{s}}(t) = \mathbf{A}\mathbf{s}(t) + \mathbf{B}\mathbf{u}(t), \quad \mathbf{s}(T_0) = \mathbf{s}_0 \quad (1)$$

where  $\mathbf{A}$  and  $\mathbf{B}$  are known matrices of constant parameters [12]. From the actuator limits, the control vector is subject to the inequality constraint

$$-\mathbf{1} \leq \mathbf{u}(t) \leq \mathbf{1} \quad (2)$$

where  $\mathbf{1}$  denotes a  $2n \times 1$  vector of 1s, and the physical scaling parameters are absorbed into  $\mathbf{B}$ .

Assuming every sensor in the network is a passive, omnidirectional sensor, the field-of-view (FoV) can be represented by a disk  $C_i(t) = \mathcal{C}[\mathbf{s}_i(t), r_i]$ , with constant radius or *effective range*  $r_i \in \mathbb{R}$ , and centered at  $\mathbf{s}_i$ . Then, the probability that the  $i$ th sensor detects a target at  $\mathbf{x}(t) \in \mathcal{A}$ , at time  $t$ , can be described by the Boolean detection model [13]–[16]

$$P_b[\mathbf{s}_i(t), \mathbf{x}(t)] = \begin{cases} 0 & : \|\mathbf{s}_i(t) - \mathbf{x}(t)\| > r_i \\ 1 & : \|\mathbf{s}_i(t) - \mathbf{x}(t)\| \leq r_i \end{cases}, \quad 1 \leq i \leq n \quad (3)$$

where  $\|\cdot\|$  denotes the  $L_2$ -norm.

Manuscript received December 6, 2013; revised August 24, 2014 and January 13, 2015; accepted January 24, 2015. Recommended by Associate Editor J. H. Braslavsky.

The authors are with the Laboratory for Intelligent Systems and Controls (LISC), Duke University, Durham, NC 27708-0005 USA (e-mail: hongchuan.wei@duke.edu; sferrari@duke.edu).

Color versions of one or more of the figures in this paper are available online at <http://ieeexplore.ieee.org>.

Digital Object Identifier 10.1109/TAC.2015.2405292

TABLE I  
MARKOV MOTION MODEL PROBABILITY DENSITY FUNCTIONS (pdfs)

Interval ( $t_j, t_{j+1}$ ] (s)	Heading PDF $f_{\Theta_j}(\theta_j)$	Velocity PDF $f_{V_j}(v_j)$
(0, 10] (s) ( $j = 1$ )	$\mathcal{U}(-\pi/3, -\pi/6)$	$\mathcal{U}(13, 16)$
(10, 20] (s) ( $j = 2$ )	$\mathcal{U}(-\pi/16, \pi/16)$	$\mathcal{U}(18, 22)$
(20, 30] (s) ( $j = 3$ )	$\mathcal{U}(\pi/2, 2\pi/3)$	$\mathcal{U}(11, 14)$
(30, 40] (s) ( $j = 4$ )	$\mathcal{U}(-\pi/2, -\pi/3)$	$\mathcal{U}(21, 26)$
(40, 50] (s) ( $j = 5$ )	$\mathcal{U}(-\pi/8, \pi/8)$	$\mathcal{U}(10, 14)$

85 This technical note considers the problem of planning the sensor  
86 motion based on the Markov transition probability density functions  
87 (pdfs) that are routinely outputted by tracking and estimation routines  
88 for assimilating distributed sensor measurements [7]. Markov motion  
89 models assume that the target obeys the kinematic equations

$$\dot{\mathbf{x}}(t) \triangleq \begin{bmatrix} \dot{x}(t) \\ \dot{y}(t) \end{bmatrix} = \begin{bmatrix} v(t) \cos \theta(t) \\ v(t) \sin \theta(t) \end{bmatrix}, \quad t \in (T_0, T_f] \quad (4)$$

90 where  $v(t)$  is the target velocity, and  $\theta(t)$  is the target heading. It  
91 is also assumed that the target heading and velocity remain constant  
92 during  $m$  subintervals  $(t_j, t_{j+1}]$ ,  $j = 1, \dots, m$ , that are an exact cover  
93 of  $(T_0, T_f]$ . At any time  $t_j$ ,  $j = 1, \dots, m$ , the target may change  
94 its heading and velocity and, thus,  $t_1, \dots, t_m$  are referred to as  
95 *maneuvering times*. Now, letting  $\mathbf{x}_j \triangleq \mathbf{x}(t_j)$ ,  $\theta_j \triangleq \theta(t_j)$ ,  $v_j \triangleq v(t_j)$ ,  
96 and integrating (4) over time yields the target motion model

$$\mathbf{x}_{j+1} = \mathbf{x}_j + [v_j \cos \theta_j \quad v_j \sin \theta_j]^T \Delta t_j, \quad j = 1, \dots, m \quad (5)$$

97 where  $\Delta t_j \triangleq t_{j+1} - t_j$ .

98 Because the target motion is unknown *a priori*, the target position,  
99 speed, and heading, are all viewed as independent, continuous random  
100 variables. Let  $\mathbf{X}_j$  denote the random target position at  $t_j$ ,  $\Theta_j$  denote  
101 the random target heading in  $(t_j, t_{j+1}]$ , and  $V_j$  denote the random  
102 target speed in  $(t_j, t_{j+1}]$ . Then,  $\mathbf{X}_j$  can take any value  $\mathbf{x}_j \in \mathcal{A}$  with  
103 a probability defined by the pdf  $f_{\mathbf{x}_j}(\mathbf{x}_j)$ ,  $\Theta_j$  can take any value  
104  $\theta_j \in [\theta_{\min}, \theta_{\max}]$  with a probability defined by the pdf  $f_{\Theta_j}(\theta_j)$ , and  
105  $V_j$  can take any value  $v_j \in [v_{\min}, v_{\max}]$  with a probability defined by  
106 the pdf  $f_{V_j}(v_j)$ . From (5), the set of Markov parameters at the  $j$ th time  
107 interval,  $\mathcal{M}_j \triangleq \{\mathbf{x}_j, \theta_j, v_j\}$ , depends only on the motion parameters  
108 at the previous time interval, or  $\mathcal{M}_{j-1}$ . Thus, it can be easily shown  
109 that the sequence  $\{\mathcal{M}_1, \dots, \mathcal{M}_m\}$  is a Markov chain [17], and  $\mathcal{M}_j$   
110 is a set of Markov motion parameters that can be described by the  
111 pdfs  $f_{\mathbf{x}_j}(\mathbf{x}_j)$ ,  $f_{\Theta_j}(\theta_j)$ , and  $f_{V_j}(v_j)$ ,  $j = 1, \dots, m$ . For simplicity, in  
112 this technical note, the maneuvering time(s),  $t_j$ , are assumed known *a*  
113 *priori* for all  $j$ .

114 An example of Markov motion realization (target track) obtained  
115 from the pdfs in Table I is shown in Fig. 1, and an example of sensor  
116 trajectory and FoV are plotted in Fig. 2. Since both the target and the  
117 sensor move over time, a detection can only occur when the target  
118 track intersects the region spanned by the sensor FoV in  $\Omega \triangleq \mathcal{A} \times$   
119  $(T_0, T_f] \subset \mathbb{R}^3$ . We are now ready to state the problem addressed in  
120 this technical note.

121 **Problem II.1—Sensor Network Motion Planning (SNMP):** Given  
122 the pdfs of the Markov parameters  $\mathcal{M}_j$ ,  $j = 1, \dots, m$ , for a target  
123 traversing the RoI  $\mathcal{A} \subset \mathbb{R}^2$ , find the network state and control tra-  
124 jectories,  $\mathbf{s}^*(t)$  and  $\mathbf{u}^*(t)$ , such that the probability of detection is  
125 maximized over  $(T_0, T_f]$ .

### III. PROBABILITY OF TRACK DETECTION

127 This section extends the results in [6] to mobile sensor networks  
128 and derives an objective function representing the probability of track

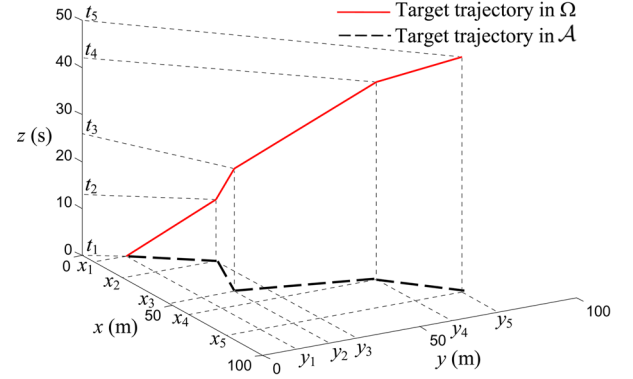


Fig. 1. Example of target trajectory realization sampled from Markov motion model in Table I.

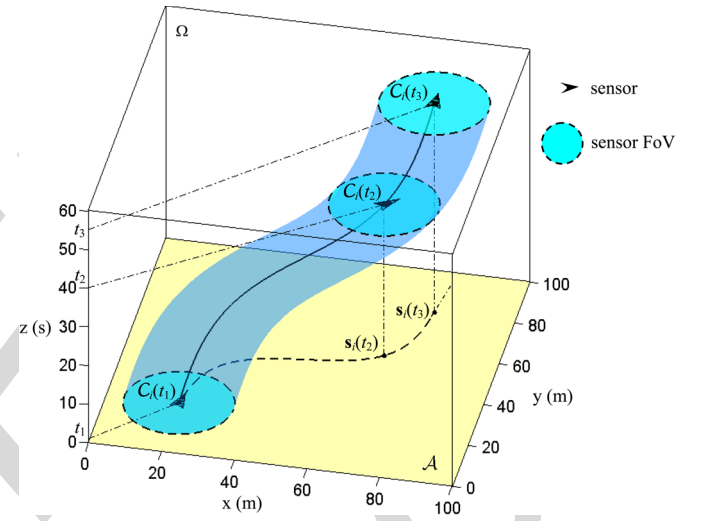


Fig. 2. Example of sensor trajectory and sensor FoV plotted at three moments in time  $t_1 = 1(s)$ ,  $t_2 = 40(s)$ , and  $t_3 = 55(s)$ .

129 detection as a function of the time-varying network state,  $\mathbf{s}(t)$ . Then,  
130 the detection probability function can be optimized subject to the  
131 network dynamic equation (1) using optimal control theory. From the  
132 detection model (3), the  $i$ th sensor has a nonzero probability to detect  
133 a target if and only if  $\|\mathbf{x}(t) - \mathbf{s}_i(t)\| \leq r_i$ . It can be shown that, as the  
134  $i$ th sensor moves along a trajectory  $\mathbf{s}_i(t)$ , the set of all tracks detected  
135 is contained by a time-varying three-dimensional coverage cone in  $\Omega$   
136 defined according to the following lemma:

**Lemma III.1:** The  $i$ th coverage cone defined as

$$K_i(t) = \{[xyz]^T \in \mathbb{R}^3 \mid t_j < z \leq t_{j+1},$$

$$\left\| [x \ y]^T - \frac{(z - t_j)}{(t - t_j)} [\mathbf{s}_i(t) - \mathbf{x}_j] - \mathbf{x}_j \right\| \leq \frac{(z - t_j)}{(t - t_j)} r_i \} \quad (6)$$

137 contains the set of all target tracks that intersect the  $i$ th sensor FoV,  
138  $C_i(t)$ , at any time  $t \in (t_j, t_{j+1}]$ .

**Proof:** Let the directed line segment  $\mathbf{m}_j(t) \subset \Omega$  represent a  
140 target track as it evolves from time  $t_j$  to  $t$ , such that

$$\mathbf{m}_j(t) = \left\{ \mathbf{y} \in \mathbb{R}^3 \mid \mathbf{y} = \mathbf{z}_j + \alpha \begin{pmatrix} \mathbf{x}^T(t) \\ t \end{pmatrix} - \mathbf{z}_j, \alpha \in (0, 1] \right\} \quad (7)$$

142 where  $\mathbf{z}_j = [\mathbf{x}_j^T \ t_j]^T$  is the segment origin in an inertial frame  $\mathcal{F}_\Omega$   
143 embedded in  $\Omega$ . Then, any point  $\mathbf{a} \in \mathbf{m}_j(t)$ , represented as a con-  
144 stant three-dimensional vector  $\mathbf{a} = [a_x \ a_y \ a_z]^T$ , obeys the equality,

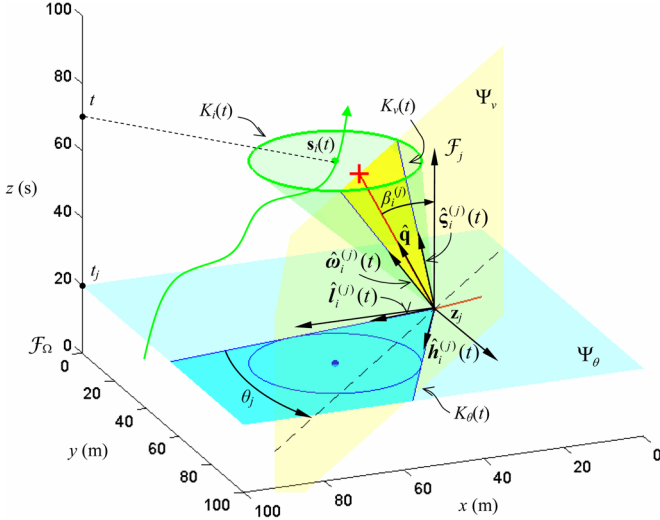


Fig. 3. Time-varying coverage cone (green) with its heading-cone (cyan) and velocity-cone (yellow) representations (adapted from [6]).

145  $[a_x \ a_y]^T = (a_z - t_j)[\mathbf{x}(t) - \mathbf{x}_j]/(t - t_j) + \mathbf{x}_j$ . From (3), a target at  
146  $\mathbf{a}$  is detected if and only if

$$\left\| [a_x \ a_y]^T - \frac{(a_z - t_j)}{(t - t_j)} [\mathbf{s}_i(t) - \mathbf{x}_j] - \mathbf{x}_j \right\| \leq \frac{(a_z - t_j)}{(t - t_j)} r_i. \quad (8)$$

147 Thus, from (6), any point on  $\mathbf{m}_j(t)$  contained by  $\mathcal{C}_i(t)$  must be  
148 contained by the coverage cone, and thus  $\mathbf{m}_j(t) \in K_i(t)$ . ■

149 As illustrated in Fig. 3, the above lemma extends the definition of  
150 the *fixed* spatio-temporal coverage cone presented in [6] to a *time-*  
151 *varying* coverage cone  $K_i(t)$  that is a function of the sensor trajectory  
152  $\mathbf{s}_i(t)$ . Because  $K_i(t)$  is a circular cone that is possibly oblique, a  
153 Lebesgue measure of the tracks contained by  $K_i(t)$  can be obtained  
154 by considering the pair of two-dimensional (2-D) cones, referred to as  
155 *heading cone* and *velocity cone* [6], and reviewed in the next section.

#### 156 A. Heading and Velocity Cones Representation

157 The heading cone, denoted by  $K_\theta(t)$ , contains all target headings  
158 that lead to a detection by the  $i$ th sensor at any time  $t \in (t_j, t_{j+1}]$  and,  
159 thus, it is obtained from the projection of  $K_i(t)$  onto the heading plane

$$\Psi_\theta \triangleq \{[x \ y \ z]^T \in \Omega \mid z = t_j\}. \quad (9)$$

160 Because  $K_\theta$  is a 2-D cone, it can be expressed as a linear combination  
161 of two unit vectors in  $\Psi_\theta$

$$\begin{aligned} \hat{\mathbf{h}}_{ij}(t) &= \begin{bmatrix} \cos \alpha_{ij}(t) & -\sin \alpha_{ij}(t) \\ \sin \alpha_{ij}(t) & \cos \alpha_{ij}(t) \\ 0 & 0 \end{bmatrix} \hat{\mathbf{d}}_{ij}(t) \triangleq \begin{bmatrix} \cos \phi_{ij}(t) \\ \sin \phi_{ij}(t) \\ 0 \end{bmatrix} \\ \hat{\mathbf{l}}_{ij}(t) &= \begin{bmatrix} \cos \alpha_{ij}(t) & \sin \alpha_{ij}(t) \\ -\sin \alpha_{ij}(t) & \cos \alpha_{ij}(t) \\ 0 & 0 \end{bmatrix} \hat{\mathbf{d}}_{ij}(t) \triangleq \begin{bmatrix} \cos \psi_{ij}(t) \\ \sin \psi_{ij}(t) \\ 0 \end{bmatrix} \end{aligned}$$

162 where

$$\begin{aligned} \hat{\mathbf{d}}_{ij}(t) &= [\mathbf{s}_i(t) - \mathbf{x}_j] / \|\mathbf{s}_i(t) - \mathbf{x}_j\| \\ \alpha_{ij}(t) &= \sin^{-1}(r_i / \|\mathbf{s}_i(t) - \mathbf{x}_j\|) \end{aligned}$$

163 such that the heading cone defined with respect to a local coordinate  
164 frame  $\mathcal{F}_j$  is

$$K_\theta[\mathbf{s}_i(t), \mathbf{z}_j] \triangleq \{c_1 \hat{\mathbf{h}}_{ij}(t) + c_2 \hat{\mathbf{l}}_{ij}(t) \mid c_1, c_2 \geq 0\}. \quad (10)$$

Examples of heading cone and heading plane are illustrated in Fig. 3, 165  
along with the unit vector representation. 166

The velocity cone, denoted by  $K_v(t)$ , contains all target speeds that 167  
lead to a detection by the  $i$ th sensor at any time  $t \in (t_j, t_{j+1}]$  and, thus, 168  
it is obtained from the intersection of  $K_i(t)$  with the velocity plane 169

$$\Psi_v \triangleq \left\{ \begin{bmatrix} x \\ y \\ z \end{bmatrix} \in \Omega \mid \begin{bmatrix} \sin \theta_j \\ \cos \theta_j \end{bmatrix}^T \begin{bmatrix} x \\ -y \end{bmatrix} = \begin{bmatrix} \sin \theta_j \\ \cos \theta_j \end{bmatrix} \mathbf{x}_j, z \geq t_j \right\}. \quad (11)$$

Similarly to the heading cone,  $K_v$  can be represented by two unit 170  
vectors 171

$$\begin{aligned} \hat{\mathbf{s}}_{ij}(t) &= [\sin \eta_{ij}(t) \cos \theta_j \quad \sin \eta_{ij}(t) \sin \theta_j \quad \cos \eta_{ij}(t)]^T \\ \hat{\omega}_{ij}(t) &= [\sin \mu_{ij}(t) \cos \theta_j \quad \sin \mu_{ij}(t) \sin \theta_j \quad \cos \mu_{ij}(t)]^T \end{aligned}$$

where 172

$$\begin{aligned} \eta_{ij}(t), \mu_{ij}(t) &= \tan^{-1} \left[ \frac{1}{t - t_j} ([\cos \theta_j \sin \theta_j](\mathbf{s}_i(t) - \mathbf{x}_j) \right. \\ &\quad \left. \mp \sqrt{r_i^2 - ([\sin \theta_j - \cos \theta_j](\mathbf{s}_i(t) - \mathbf{x}_j))^2} \right) \end{aligned}$$

such that the velocity cone in  $\mathcal{F}_j$  is 173

$$K_v[\mathbf{s}_i(t), \mathbf{z}_j] \triangleq \{c_1 \hat{\mathbf{s}}_{ij}(t) + c_2 \hat{\omega}_{ij}(t) \mid c_1, c_2 \geq 0\}. \quad (12)$$

Then, the pair of cones  $\{K_\theta(t), K_v(t)\}$ , defined in (10) and (12), 174  
can be used to represent all tracks in  $K_i(t)$ , as summarized by the 175  
following lemma (adapted from [6]). 176

**Lemma III.2:** A target track  $\mathbf{m}_j(t)$  is contained by the coverage 177  
cone  $K_i(t)$  if and only if its projection in  $\Psi_\theta$  is contained by the 178  
heading cone  $K_\theta(t)$ , and its projection in  $\Psi_v$  is contained by the 179  
corresponding velocity cone  $K_v(t)$ . 180

The proof of Lemma III.2 is a simple extension of the proof in [6]. 181

#### 182 B. SNMP Objective Function

The extremals of the heading and velocity cones presented in the 183  
previous section determine upper and lower bounds for the target 184  
heading angle and speed, respectively, that lead to a detection by 185  
the  $i$ th sensor, as functions of the time-varying sensor position  $\mathbf{s}_i$ . 186  
Let the intervals  $\mathcal{H}_{ij}(t) \triangleq [\psi_{ij}(t), \phi_{ij}(t)]$  and  $\mathcal{V}_{ij}(t) \triangleq [\tan \eta_{ij}(t),$  187  
 $\tan \mu_{ij}(t)]$  respectively denote the headings and speeds contained by 188  
the heading and velocity cones. Then, the probability that the  $i$ th sensor 189  
detects the target at any time  $t \in (t_j, t_{j+1}]$  is the probability that the 190  
Markov parameters are contained by the coverage cone  $K_i(t)$  191

$$P_d(i, j, t) = \int_{\mathcal{A} \times \mathcal{H}_{ij}(t) \times \mathcal{V}_{ij}(t)} f_{\mathbf{x}_j, \Theta_j, V_j}(\mathbf{x}_j, \theta_j, v_j) d\mathbf{x}_j d\theta_j dv_j \quad (13)$$

where  $f_{\mathbf{x}_j, \Theta_j, V_j}(\cdot)$  is the joint pdf of the Markov parameters  $\mathbf{x}_j$ ,  $\theta_j$ , 192  
and  $v_j$ . Since these parameters are independent random variables, the 193  
probability of detection can be simplified to 194

$$\begin{aligned} P_d(i, j, t) &= \int_{\mathcal{A} \times \mathcal{H}_{ij}(t) \times \mathcal{V}_{ij}(t)} f_{\mathbf{x}_j}(\mathbf{x}_j) f_{\Theta_j}(\theta_j) f_{V_j}(v_j) d\mathbf{x}_j d\theta_j dv_j \\ &= \int_{\mathbf{x}_j \in \mathcal{A}} f_{\mathbf{x}_j}(\mathbf{x}_j) \int_{\psi_{ij}(t)}^{\phi_{ij}(t)} f_{\Theta_j}(\theta_j) \int_{\tan \eta_{ij}(t)}^{\tan \mu_{ij}(t)} f_{V_j}(v_j) dv_j d\theta_j d\mathbf{x}_j \\ &\quad \forall t \in (t_j, t_{j+1}]. \end{aligned} \quad (14)$$

It can be seen that using the 2-D coverage cones reduces the region of integration from  $\Omega$  to the product space  $\mathcal{A} \times \mathcal{H}_{ij}(t) \times \mathcal{V}_{ij}(t)$ , and thus reduces the computation required to evaluate the detection probability. Then, the objective function for the SNMP problem can be obtained by integrating over time the probability of independent sensor detections by the  $n$  sensors for all  $m$  time intervals, as follows:

$$\begin{aligned} J &= -\frac{1}{n} \sum_{i=1}^n \sum_{j=1}^m \int_{t_j}^{t_{j+1}} P_d(i, j, t) dt \\ &= -\frac{1}{n} \sum_{i=1}^n \sum_{j=1}^m \int_{t_j}^{t_{j+1}} \int_{\mathcal{A}} f_{\mathbf{x}_j}(\mathbf{x}_j) \int_{\psi_{ij}(t)}^{\phi_{ij}} (t) f_{\Theta_j}(\theta_j) \\ &\quad \times \int_{\tan \mu_{ij}(t)}^{\tan \nu_{ij}(t)} f_{V_j}(v_j) dv_j d\theta_j d\mathbf{x}_j dt. \end{aligned} \quad (15)$$

The above objective function is to be optimized subject to the network dynamics (1) and the inequality constraints on the network state and control given by  $\mathbf{c}[\mathbf{s}(t)] \leq \mathbf{0}_{(n-1)n \times 1}$  and (2), respectively. The inequality constraint on the state is defined as the vector function  $\mathbf{c} = [c_{12} \cdots c_{il} \cdots c_{n(n-1)}]^T$ , where

$$c_{il} \triangleq (r_i + r_l)^2 - \|\mathbf{s}_i(t) - \mathbf{s}_l(t)\|^2, \quad i, l = 1, \dots, n, \quad i \neq l$$

and is used to guarantee independent sensor detections (see [5] and references therein for a comprehensive treatment of detection theory). Therefore, the SNMP problem can be formulated as the following optimal control problem:

$$\begin{aligned} \min \quad & J \\ \text{sbj. to} \quad & \dot{\mathbf{s}}(t) = \mathbf{A}\mathbf{s}(t) + \mathbf{B}\mathbf{u}(t) \\ & \mathbf{c}[\mathbf{s}(t)] \leq \mathbf{0} \\ & -\mathbf{1} \leq \mathbf{u}(t) \leq \mathbf{1}. \end{aligned} \quad (16)$$

Because  $J$  is not quadratic, the above SNMP optimal control problem must be solved numerically for the optimal state and control trajectories  $\mathbf{s}^*(t)$  and  $\mathbf{u}^*(t)$ . Section IV derives the SNMP EL equations, and explains how their numerical solution can be obtained via VIM. The VIM numerical simulation results and complexity analysis are presented in Section V.

#### IV. OPTIMAL CONTROL SOLUTION

In order to maximize the detection probability and minimize the control usage, the SNMP objective function is chosen to be of the Lagrange type, with Lagrangian

$$\begin{aligned} \mathcal{L}[\mathbf{s}(t), \mathbf{u}(t), t] &= -\sum_{i=1}^n \sum_{j=1}^m \int_{\mathcal{A}} f_{\mathbf{x}_j}(\mathbf{x}_j) \int_{\psi_{ij}(t)}^{\phi_{ij}} (t) f_{\Theta_j}(\theta_j) \\ &\quad \times \int_{\tan \mu_{ij}(t)}^{\tan \nu_{ij}(t)} f_{V_j}(v_j) dv_j d\theta_j d\mathbf{x}_j + \alpha \mathbf{u}^T \mathbf{u}. \end{aligned} \quad (17)$$

To find the necessary conditions for optimality, the Hamiltonian

$$\begin{aligned} \mathcal{H} &\triangleq \mathcal{L}[\cdot] + \lambda^T(t) [\mathbf{A}\mathbf{s}(t) + \mathbf{B}\mathbf{u}(t)] + \gamma^T(t) \mathbf{c}[\mathbf{s}(t)] \\ &= \mathcal{H}[\mathbf{s}(t), \mathbf{u}(t), \lambda(t), \gamma(t)] \end{aligned} \quad (18)$$

is introduced, adjoining the constraints on the state and control to (17) by means of the Lagrange multipliers  $\lambda$  and  $\gamma$ .

Then, the SNMP Euler–Lagrange equations are

$$\dot{\lambda}(t) = -(\partial \mathcal{L}[\cdot] / \partial \mathbf{s})^T - \mathbf{A}^T \lambda(t) - (\partial \mathbf{c}[\cdot] / \partial \mathbf{s})^T \gamma(t) \quad (19)$$

$$\lambda(T_f) = \mathbf{0} \quad (20)$$

$$(\partial \mathcal{L}[\cdot] / \partial \mathbf{u})^T + \mathbf{B}^T \lambda(t) + (\partial \mathbf{c}[\cdot] / \partial \mathbf{u})^T \gamma(t) = \mathbf{0} \quad (21)$$

where  $\partial \mathcal{L} / \partial \mathbf{s} = [(\partial \mathcal{L} / \partial \mathbf{s}_1)^T \cdots (\partial \mathcal{L} / \partial \mathbf{s}_n)^T]^T$ . Letting  $\xi_{ij}$ ,  $\zeta_{ij} = (\psi_{ij} \mp \phi_{ij})/2$ , the partial derivatives of the Lagrangian with respect to the state can be approximated as

$$\frac{\partial \mathcal{L}}{\partial \mathbf{s}_i} \approx \left[ \rho \int_{\mathcal{A}} \{ f_{\mathbf{x}_j}(\mathbf{x}_j) \xi_{ij}(\mathbf{s}_i, \mathbf{x}_j) \sin[\zeta_{ij}(\mathbf{s}_i, \mathbf{x}_j)] \} d\mathbf{x}_j \right] \triangleq \mathbf{g}_i[\mathbf{s}_i(t)] \quad (22)$$

where  $\rho = -8 \ln(\pi/2) / (|V_j| |\Theta_j| (t - t_j))$  and  $|\cdot|$  denotes the variable's range, and the partial derivative of the Lagrangian with respect to the control is  $\partial \mathcal{L} / \partial \mathbf{u} = \alpha \mathbf{u}^T(t)$ . Since  $\partial \mathbf{c} / \partial \mathbf{u} = \mathbf{0}$ , (21) simplifies to  $\alpha \mathbf{u}(t) + \mathbf{B}^T \lambda = \mathbf{0}$  and, thus

$$\mathbf{u}(t) = -\frac{1}{\alpha} \mathbf{B}^T \lambda(t). \quad (23)$$

Now, from the transition matrix solution of the state-space form (1),  $\mathbf{s}(t) = e^{\mathbf{A}(t-T_0)} \mathbf{s}_0 + \int_{T_0}^t \mathbf{B} \mathbf{u}(\tau) d\tau$ , and, thus, from (23) it follows that

$$\mathbf{s}(t) = e^{\mathbf{A}(t-T_0)} \mathbf{s}_0 - \frac{1}{\alpha} \int_{T_0}^t \mathbf{B} \mathbf{B}^T \lambda(\tau) d\tau. \quad (24)$$

Because  $\gamma = \mathbf{0}$  when  $\mathbf{c}[\mathbf{s}(t)] \neq \mathbf{0}$ , it also follows from (24) that the first optimality condition (19) can be simplified to

$$\dot{\lambda}(t) = -\mathbf{g}[\mathbf{s}(t)] \left( \int_0^t \mathbf{B} \mathbf{B}^T \lambda(\tau) d\tau \right) - \mathbf{A}^T \lambda(t) \quad (25)$$

where the vector function  $\mathbf{g}[\cdot] \triangleq [\mathbf{g}_1^T[\cdot] \cdots \mathbf{g}_n^T[\cdot]]$  is defined according to (22). Thus, (25) represents a set of integro-differential equations with boundary conditions (20).

Many algorithms have been developed for solving integro-differential equations, including the Adomian decomposition method [18], the homotopy perturbation method [19], and the VIM [20]. In this technical note, VIM is chosen to solve (25) because its intermediate approximations are known to converge rapidly to an accurate solution. VIM starts with a linear trial function and obtains higher order terms iteratively as follows:

$$\begin{aligned} \lambda^{(\ell+1)}(t) &= \lambda^{(\ell)}(t) \\ &\quad - \int_{T_0}^t \left\{ \mathbf{A}^T \lambda^{(\ell)}(\sigma) - \mathbf{g}[\mathbf{s}(t)] \left[ \int_{T_0}^{\sigma} \mathbf{B} \mathbf{B}^T \lambda^{(\ell)}(\tau) d\tau \right] \right\} d\sigma \end{aligned} \quad (26)$$

where the superscript  $\ell$  denotes the  $\ell$ th-order approximation.

By exploiting the integro-differential structure of the EL equations, VIM can significantly reduce computational complexity when compared to direct methods of solution. In direct methods, the dynamic equation and objective function are discretized and transcribed into an NLP that, typically, is solved using sequential quadratic programming (SQP) [21]. The computational complexity of SQP direct methods is  $O(n^3 K^3 M)$ , where  $n$  is the number of sensors,  $K$  is the number of



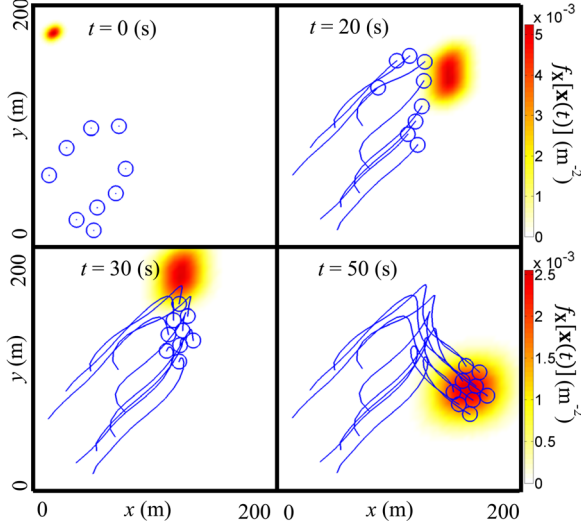


Fig. 4. Optimal sensor trajectories for  $n = 9$  and  $r_i = 6$  (m), given the target motion model in Table I.

254 collocation points, and  $M$  is the number of iterations required for  
 255 convergence [21]. The indirect VIM, on the other hand, requires a  
 256 computation time of  $O(nK^2)$  to evaluate (26) using Euler integration.  
 257 Therefore, the computation complexity for VIM is  $O(nK^2M)$ , where  
 258 in practice  $M$  is quite small. Therefore, the VIM solution is efficient  
 259 for mobile sensor networks with a few dozen sensors. For larger  $n$ ,  
 260 efficient solutions can be obtained by combining the results in this  
 261 technical note with the distributed optimal control approach presented  
 262 in [22].

## V. SIMULATION RESULTS

264 Consider the Markov motion model in Table I for a target traversing  
 265 the RoI over a time interval  $(T_0, T_f] = (0, 50](s)$ , where  $m = 5$ . At  
 266  $t_1 = T_0 = 0$  (s), the pdf of the target position,  $f_{\mathbf{x}_1}(\mathbf{x}_1)$ , is a 2-D mul-  
 267 tivariate Gaussian distribution, denoted by  $\mathcal{N}(\boldsymbol{\mu}, \boldsymbol{\Sigma})$ , with mean  $\boldsymbol{\mu} =$   
 268  $[20 \ 180]^T$  (m) and covariance matrix  $\boldsymbol{\Sigma} = \text{diag}([10 \ 10])$  (m<sup>2</sup>),  
 269 where,  $\text{diag}(\cdot)$  denotes an operator that places a row vector on the  
 270 diagonal of a zero matrix. The heading and velocity pdfs are uniform  
 271 distributions, denoted by  $\mathcal{U}(a, b)$ , with support  $[a, b]$ , as shown in  
 272 Table I. Then, the pdfs of  $\mathbf{x}_2, \dots, \mathbf{x}_5$ , can be computed recursively,  
 273 as shown in [6].

274 Simulation results are presented for two example cases, one network  
 275 with  $n = 9$  and  $r_i = 6$  (m) (Fig. 4), and one network with  $n = 20$   
 276 and  $r_i = 5$  (m) (Fig. 5). Figs. 4 and 5 show the sensor trajectories and  
 277 FoVs, and the pdf of the target position, at four sample instants in time.  
 278 It can be seen that by the geometric transversals approach the sensors  
 279 plan their motion such that the detection probability in  $(T_0, T_f]$  is  
 280 maximized. The optimal control histories of a randomly chosen sensor  
 281 (red arrow in Fig. 5) are plotted in Fig. 6 to illustrate that control  
 282 inputs obtained by this approach are smooth and obey the desired  
 283 bounds in (2).

284 The effectiveness of the geometric transversals approach is illus-  
 285 trated by comparing the probability of detection obtained by the  
 286 network in Fig. 5 to that obtained by potential field, greedy, uniform  
 287 grid, and random algorithms. In potential field [23], the pdf of the  
 288 target position is used to build an attractive potential, and a repulsive  
 289 force  $f_r = -c_r / \|\mathbf{s}_i(t) - \mathbf{s}_j(t)\|^2$  is used to prevent collisions between  
 290 sensors, where  $c_r = 1$  [23]. The greedy algorithm proposed in [24]  
 291 places the sensors at  $n$  fixed locations, such that the network cover-  
 292 age is maximized while retaining line-of-sight relationships between

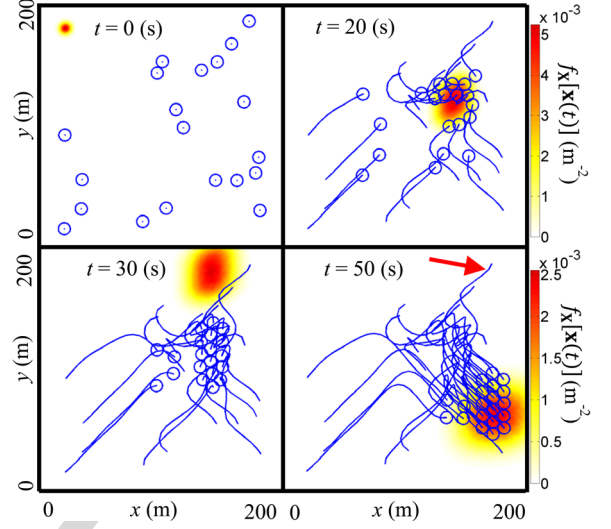


Fig. 5. Optimal sensor trajectories for  $n = 20$  and  $r_i = 5$  (m), given the target motion model in Table I.

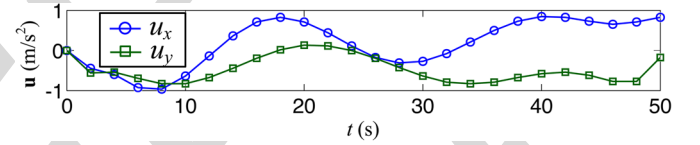


Fig. 6. Optimal control histories of one sensor chosen at random from the network in Fig. 5 (as shown by red arrow).

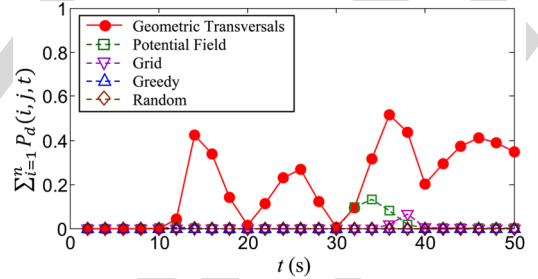


Fig. 7. Performance comparison for sensor network in Fig. 5, with  $n = 20$ ,  $r_i = 5$  (m), and the target motion model in Table I.

293 sensors. The grid and random algorithms proposed in [25] place the  
 294 sensors at  $n$  fixed locations in  $\mathcal{A}$  according to a uniformly spaced grid  
 295 or by sampling a uniform distribution.

296 The results in Fig. 7 are representative of extensive simulations  
 297 performed using different sensor networks, target models, and initial  
 298 conditions. Because the network performance is highly sensitive to  
 299 initial conditions, the average probability of detection, denoted by  $P_e$ ,  
 300 is computed by considering over 100 initial conditions, sampled uni-  
 301 formly at random from the RoI, holding network and target parameters  
 302 constant. The mean performance ( $P_e$ ) and three standard deviations  
 303 (SDs) obtained by the five algorithms are plotted in Fig. 8 and show  
 304 that the geometric transversals approach significantly outperforms  
 305 other algorithms over the entire time interval  $(T_0, T_f]$ .

## VI. SUMMARY AND CONCLUSIONS

306 This technical note presents a geometric transversals approach for  
 307 planning the motion of a mobile sensor network such that its detection  
 308 probability is maximized over time. By this approach, the approach  
 309 derives a track coverage objective function in closed form, based on  
 310

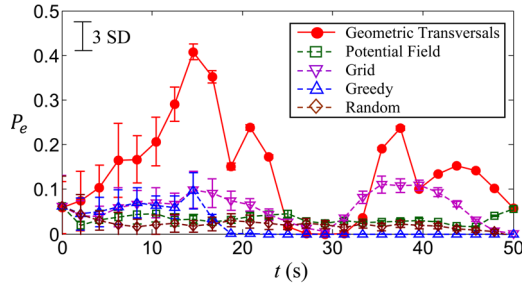


Fig. 8. Probability of detection averaged over 100 initial conditions for  $n = 20$ ,  $r_s = 5$  (m), and the target motion model in Table I.

the transition pdfs of the target Markov motion model. By this novel approach, the probability of detection can be optimized subject to the sensor kinodynamic equations, and inequality constraints on the sensor state and control. The necessary conditions for optimality are derived and reduced to a set of integro-differential equations that are solved numerically using a variational iteration method. The results show that by this approach the computational complexity is significantly reduced compared to a direct method, and the detection probability is significantly increased compared to existing potential field, greedy, grid, or random algorithms.

#### REFERENCES

- [1] I. F. Akyildiz, W. Su, Y. Sankarasubramaniam, and E. Cayirci, "Wireless sensor networks: A survey," *Comput. Netw.*, vol. 38, no. 4, pp. 393–422, 2002.
- [2] D. Chen and P. K. Varshney, "Qos support in wireless sensor networks: A survey," in *Proc. Int. Wireless Netw. Conf.*, 2004, vol. 233.
- [3] X. R. Li and V. P. Jilkov, "Survey of maneuvering target tracking. part i. dynamic models," *IEEE Trans. Aerosp. Electron. Syst.*, vol. 39, no. 4, pp. 1333–1364, 2003.
- [4] K. Baumgartner and S. Ferrari, "A geometric transversal approach to analyzing track coverage in sensor networks," *IEEE Trans. Comput.*, vol. 57, no. 8, pp. 1113–1128, Aug. 2008.
- [5] T. A. Wettergren, "Performance of search via track-before-detect for distributed sensor networks," *IEEE Trans. Aerosp. Electron. Syst.*, vol. 44, no. 1, pp. 314–325, Jan. 2008.
- [6] H. Wei and S. Ferrari, "A geometric transversals approach to analyzing the probability of track detection for maneuvering targets," *IEEE Trans. Comput.*, vol. 63, no. 11, pp. 2633–2646, Nov. 2013.
- [7] Y. Bar-Shalom and X. R. Li, *Multitarget-Multisensor Tracking: Principles and Techniques*. Storrs, CT, USA: Yaakov Bar-Shalom, 1995.
- [8] P. Fiorini and Z. Shiller, "Motion planning in dynamic environments using velocity obstacles," *Int. J. Robot. Res.*, vol. 17, no. 7, pp. 760–772, 1998.
- [9] H. Wei, W. Lu, P. Zhu, G. Huang, J. Leonard, and S. Ferrari, "Optimized visibility motion planning for target tracking and localization," in *Proc. IEEE/RSJ Int. Conf. Intell. Robots Syst. (IROS 2014)*, 2014, pp. 76–82.
- [10] J. Betts, "Survey of numerical methods for trajectory optimization," *J. Guid., Control, Dynam.*, vol. 21, no. 2, pp. 193–207, 1998.
- [11] Y. Bar-Shalom and X.-R. Li, *Estimation and Tracking: Principles, Techniques, Software*, vol. 393. Norwood, MA, USA: Artech House, 1993.
- [12] H. Wei, W. Ross, S. Varisco, P. Krief, and S. Ferrari, "Modeling of human driver behavior via receding horizon and artificial neural network controllers," in *Proc. IEEE Ann. Conf. Decision Control (CDC)*, Florence, Italy, Dec. 2013, pp. 6778–6785.
- [13] B. Liu and D. Towsley, "A study of the coverage of large-scale sensor networks," in *Proc. IEEE Int. Mobile Ad-hoc Sensor Syst. Conf.*, 2004, pp. 475–483.
- [14] H. Wei, W. Lu, and S. Ferrari, "An information value function for nonparametric gaussian processes," in *Proc. Neural Inform. Process. Syst. Conf.*, Lake Tahoe, NV, USA, 2012.
- [15] J. Yick, B. Mukherjee, and D. Ghosal, "Wireless sensor network survey," *Comput. Netw.*, vol. 52, no. 12, pp. 2292–2330, 2008.
- [16] H. Wei, W. Lu, P. Zhu, S. Ferrari, R. H. Klein, S. Omidshafiei, and J. P. How, "Camera control for learning nonlinear target dynamics via bayesian nonparametric dirichlet-process gaussian-process (DP-GP) models," in *Proc. IEEE/RSJ Int. Intell. Robots Syst. Conf. (IROS 2014)*, pp. 95–102.
- [17] S. Meyn and R. L. Tweedie, *Markov Chains and Stochastic Stability*, 2nd ed. New York, NY, USA: Cambridge Univ. Press, 2009, ser. Cambridge Mathematical Library.
- [18] G. Adomian, "A review of the decomposition method and some recent results for nonlinear equations," *Mathemat. Comput. Modell.*, vol. 13, no. 7, pp. 17–43, 1990.
- [19] J.-H. He, "Homotopy perturbation technique," *Comput. Methods Appl. Mech. Eng.*, vol. 178, no. 3, pp. 257–262, 1999.
- [20] B. Neta, "Numerical solution of a nonlinear integro-differential equation," *J. Mathemat. Anal. Appl.*, vol. 89, no. 2, pp. 598–611, 1982.
- [21] M. J. D. Powell, "A fast algorithm for nonlinearly constrained optimization calculations," *Numer. Anal.*, vol. 630, 1978.
- [22] G. Foderaro, S. Ferrari, and T. Wettergren, "Distributed optimal control for multi-agent trajectory optimization," *Automatica*, vol. 50, pp. 149–154, 2014.
- [23] S. S. Ge and Y. J. Cui, "Dynamic motion planning for mobile robots using potential field method," *Auton. Robots*, vol. 13, no. 3, pp. 207–222, 2002.
- [24] A. Howard, M. J. Matarí, and G. S. Sukhatme, "An incremental self-deployment algorithm for mobile sensor networks," *Auton. Robots*, vol. 13, pp. 113–126, 2002.
- [25] H. Gonzales-Banos and J. C. Latombe, "Robot motion planning with uncertainty in control and sensing," in *Proc. 17th Ann. Symp. Computational Geom. (SCG'01)*, Boston, MA, USA, 2001.

## AUTHOR QUERY

NO QUERY.

IEEE  
Proof

# A Geometric Transversals Approach to Sensor Motion Planning for Tracking Maneuvering Targets

Hongchuan Wei, *Student Member, IEEE*, and Silvia Ferrari, *Senior Member, IEEE*

**Abstract**—This technical note presents a geometric transversals approach for representing the probability of track detection as an analytic function of time and target motion parameters. By this approach, the optimization of the detection probability subject to sensor kinodynamic constraints can be formulated as an optimal control problem. Using the proposed detection probability function, the necessary conditions for optimality can be derived using calculus of variations, and solved numerically using a variational iteration method (VIM). The simulation results show that sensor state and control trajectories obtained by this approach bring about a significant increase in detection probability compared to existing strategies, and require a computation that is significantly reduced compared to direct methods.

**Index Terms**—Detection theory, geometric transversals, mobile sensor networks, optimal control, target tracking, track coverage.

## I. INTRODUCTION

The problem of tracking moving targets by means of a mobile sensor network is relevant to a wide range of applications, including environmental and atmospheric monitoring, security and surveillance, tracking of endangered species, and condition-based diagnostics [1]–[3]. It has been previously shown that the quality-of-service (QoS) of sensor networks performing cooperative target tracking can be quantified by track coverage functions derived using geometric transversals and probability theory, assuming targets move at constant speed and heading in the region-of-interest (RoI) [4], [5].

Recently, the geometric transversals approach in [4] was extended to maneuvering targets described by Markov motion models and used to optimize the detection probability of static sensor networks [6]. This technical note extends the results in [6] to the problem of tracking a maneuvering target by a network of omnidirectional sensors mounted on mobile vehicles, and referred to simply as *mobile sensors*. The advantage of mobile sensors over static sensors is that, over time, they can cover larger portions of the RoI, and they can plan their paths based on where targets are expected to travel to at future times. Although optimal control has been previously applied to mobile sensor networks, its applicability is often limited by the lack of suitable objective functions. This technical note shows that, using the proposed track coverage function, optimal control can be used to obtain optimality conditions and solutions for maximizing the detection probability over time, based on the probability distributions describing the target Markov motion model.

There is considerable precedence in the tracking and estimation literature for modeling target dynamics by Markov motion models [7], [8]. Using the approach presented in this technical note, mobile sensors can be controlled based on the Markov transition probability density functions (pdfs) that are routinely outputted by tracking and estimation algorithms [7], [9]. Because the track coverage function is not quadratic, the optimal control problem may be solved using direct or indirect numerical methods [10], [11]. Direct methods determine near optimal solutions by discretizing the continuous-time problem and transcribing it into a finite-dimensional nonlinear program (NLP). Thus, they may become intractable for more than a few sensors. Using the proposed track coverage function, this technical note derives necessary conditions for optimality, also known as Euler–Lagrange (EL) equations, and then determines a numerical solution using a variational iteration method (VIM) that exploits the integro-differential structure of the EL equations to reduce computational complexity. The numerical simulations show that, by this approach, the detection probability is significantly increased compared to existing potential field, greedy, grid, and random deployment algorithms.

## II. SENSOR NETWORK MOTION PLANNING (SNMP)

### PROBLEM FORMULATION

This technical note considers the problem of planning the state and control trajectories of a network of  $n$  mobile sensors that seek to cooperatively detect a moving target in a two-dimensional RoI,  $\mathcal{A} = [0, L_x] \times [0, L_y]$ , during a fixed time interval  $(T_0, T_f]$ . Each sensor is mounted on a vehicle that is assumed to obey linear and time-invariant (LTI) equations of motion. Let  $\mathbf{s}_i \in \mathcal{A}$  and  $\mathbf{u}_i \in \mathbb{R}^2$  denote the state and control of the  $i$ th vehicle, respectively, such that  $\mathbf{s} = [\mathbf{s}_1^T \dots \mathbf{s}_n^T]^T$  and  $\mathbf{u} = [\mathbf{u}_1^T \dots \mathbf{u}_n^T]^T$  denote the state and control of the sensor network, respectively. Then, the network dynamics can be represented by the state-space equation

$$\dot{\mathbf{s}}(t) = \mathbf{A}\mathbf{s}(t) + \mathbf{B}\mathbf{u}(t), \quad \mathbf{s}(T_0) = \mathbf{s}_0 \quad (1)$$

where  $\mathbf{A}$  and  $\mathbf{B}$  are known matrices of constant parameters [12]. From the actuator limits, the control vector is subject to the inequality constraint

$$-\mathbf{1} \leq \mathbf{u}(t) \leq \mathbf{1} \quad (2)$$

where  $\mathbf{1}$  denotes a  $2n \times 1$  vector of 1s, and the physical scaling parameters are absorbed into  $\mathbf{B}$ .

Assuming every sensor in the network is a passive, omnidirectional sensor, the field-of-view (FoV) can be represented by a disk  $C_i(t) = \mathcal{C}[\mathbf{s}_i(t), r_i]$ , with constant radius or *effective range*  $r_i \in \mathbb{R}$ , and centered at  $\mathbf{s}_i$ . Then, the probability that the  $i$ th sensor detects a target at  $\mathbf{x}(t) \in \mathcal{A}$ , at time  $t$ , can be described by the Boolean detection model [13]–[16]

$$P_b[\mathbf{s}_i(t), \mathbf{x}(t)] = \begin{cases} 0 & : \|\mathbf{s}_i(t) - \mathbf{x}(t)\| > r_i \\ 1 & : \|\mathbf{s}_i(t) - \mathbf{x}(t)\| \leq r_i \end{cases}, \quad 1 \leq i \leq n \quad (3)$$

where  $\|\cdot\|$  denotes the  $L_2$ -norm.

Manuscript received December 6, 2013; revised August 24, 2014 and January 13, 2015; accepted January 24, 2015. Recommended by Associate Editor J. H. Braslavsky.

The authors are with the Laboratory for Intelligent Systems and Controls (LISC), Duke University, Durham, NC 27708-0005 USA (e-mail: hongchuan.wei@duke.edu; sferrari@duke.edu).

Color versions of one or more of the figures in this paper are available online at <http://ieeexplore.ieee.org>.

Digital Object Identifier 10.1109/TAC.2015.2405292



TABLE I  
MARKOV MOTION MODEL PROBABILITY DENSITY FUNCTIONS (pdfs)

Interval ( $t_j, t_{j+1}$ ] (s)	Heading PDF $f_{\Theta_j}(\theta_j)$	Velocity PDF $f_{V_j}(v_j)$
(0, 10] (s) ( $j = 1$ )	$\mathcal{U}(-\pi/3, -\pi/6)$	$\mathcal{U}(13, 16)$
(10, 20] (s) ( $j = 2$ )	$\mathcal{U}(-\pi/16, \pi/16)$	$\mathcal{U}(18, 22)$
(20, 30] (s) ( $j = 3$ )	$\mathcal{U}(\pi/2, 2\pi/3)$	$\mathcal{U}(11, 14)$
(30, 40] (s) ( $j = 4$ )	$\mathcal{U}(-\pi/2, -\pi/3)$	$\mathcal{U}(21, 26)$
(40, 50] (s) ( $j = 5$ )	$\mathcal{U}(-\pi/8, \pi/8)$	$\mathcal{U}(10, 14)$

85 This technical note considers the problem of planning the sensor  
86 motion based on the Markov transition probability density functions  
87 (pdfs) that are routinely outputted by tracking and estimation routines  
88 for assimilating distributed sensor measurements [7]. Markov motion  
89 models assume that the target obeys the kinematic equations

$$\dot{\mathbf{x}}(t) \triangleq \begin{bmatrix} \dot{x}(t) \\ \dot{y}(t) \end{bmatrix} = \begin{bmatrix} v(t) \cos \theta(t) \\ v(t) \sin \theta(t) \end{bmatrix}, \quad t \in (T_0, T_f] \quad (4)$$

90 where  $v(t)$  is the target velocity, and  $\theta(t)$  is the target heading. It  
91 is also assumed that the target heading and velocity remain constant  
92 during  $m$  subintervals  $(t_j, t_{j+1}]$ ,  $j = 1, \dots, m$ , that are an exact cover  
93 of  $(T_0, T_f]$ . At any time  $t_j$ ,  $j = 1, \dots, m$ , the target may change  
94 its heading and velocity and, thus,  $t_1, \dots, t_m$  are referred to as  
95 *maneuvering times*. Now, letting  $\mathbf{x}_j \triangleq \mathbf{x}(t_j)$ ,  $\theta_j \triangleq \theta(t_j)$ ,  $v_j \triangleq v(t_j)$ ,  
96 and integrating (4) over time yields the target motion model

$$\mathbf{x}_{j+1} = \mathbf{x}_j + [v_j \cos \theta_j \quad v_j \sin \theta_j]^T \Delta t_j, \quad j = 1, \dots, m \quad (5)$$

97 where  $\Delta t_j \triangleq t_{j+1} - t_j$ .

98 Because the target motion is unknown *a priori*, the target position,  
99 speed, and heading, are all viewed as independent, continuous random  
100 variables. Let  $\mathbf{X}_j$  denote the random target position at  $t_j$ ,  $\Theta_j$  denote  
101 the random target heading in  $(t_j, t_{j+1}]$ , and  $V_j$  denote the random  
102 target speed in  $(t_j, t_{j+1}]$ . Then,  $\mathbf{X}_j$  can take any value  $\mathbf{x}_j \in \mathcal{A}$  with  
103 a probability defined by the pdf  $f_{\mathbf{x}_j}(\mathbf{x}_j)$ ,  $\Theta_j$  can take any value  
104  $\theta_j \in [\theta_{\min}, \theta_{\max}]$  with a probability defined by the pdf  $f_{\Theta_j}(\theta_j)$ , and  
105  $V_j$  can take any value  $v_j \in [v_{\min}, v_{\max}]$  with a probability defined by  
106 the pdf  $f_{V_j}(v_j)$ . From (5), the set of Markov parameters at the  $j$ th time  
107 interval,  $\mathcal{M}_j \triangleq \{\mathbf{x}_j, \theta_j, v_j\}$ , depends only on the motion parameters  
108 at the previous time interval, or  $\mathcal{M}_{j-1}$ . Thus, it can be easily shown  
109 that the sequence  $\{\mathcal{M}_1, \dots, \mathcal{M}_m\}$  is a Markov chain [17], and  $\mathcal{M}_j$   
110 is a set of Markov motion parameters that can be described by the  
111 pdfs  $f_{\mathbf{x}_j}(\mathbf{x}_j)$ ,  $f_{\Theta_j}(\theta_j)$ , and  $f_{V_j}(v_j)$ ,  $j = 1, \dots, m$ . For simplicity, in  
112 this technical note, the maneuvering time(s),  $t_j$ , are assumed known *a*  
113 *priori* for all  $j$ .

114 An example of Markov motion realization (target track) obtained  
115 from the pdfs in Table I is shown in Fig. 1, and an example of sensor  
116 trajectory and FoV are plotted in Fig. 2. Since both the target and the  
117 sensor move over time, a detection can only occur when the target  
118 track intersects the region spanned by the sensor FoV in  $\Omega \triangleq \mathcal{A} \times$   
119  $(T_0, T_f] \subset \mathbb{R}^3$ . We are now ready to state the problem addressed in  
120 this technical note.

121 **Problem II.1—Sensor Network Motion Planning (SNMP):** Given  
122 the pdfs of the Markov parameters  $\mathcal{M}_j$ ,  $j = 1, \dots, m$ , for a target  
123 traversing the RoI  $\mathcal{A} \subset \mathbb{R}^2$ , find the network state and control tra-  
124 jectories,  $\mathbf{s}^*(t)$  and  $\mathbf{u}^*(t)$ , such that the probability of detection is  
125 maximized over  $(T_0, T_f]$ .

### III. PROBABILITY OF TRACK DETECTION

127 This section extends the results in [6] to mobile sensor networks  
128 and derives an objective function representing the probability of track

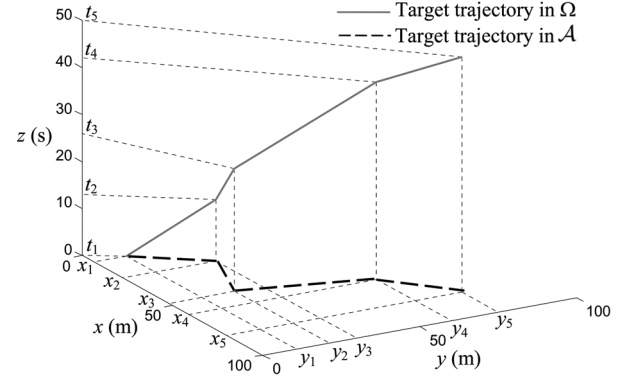


Fig. 1. Example of target trajectory realization sampled from Markov motion model in Table I.

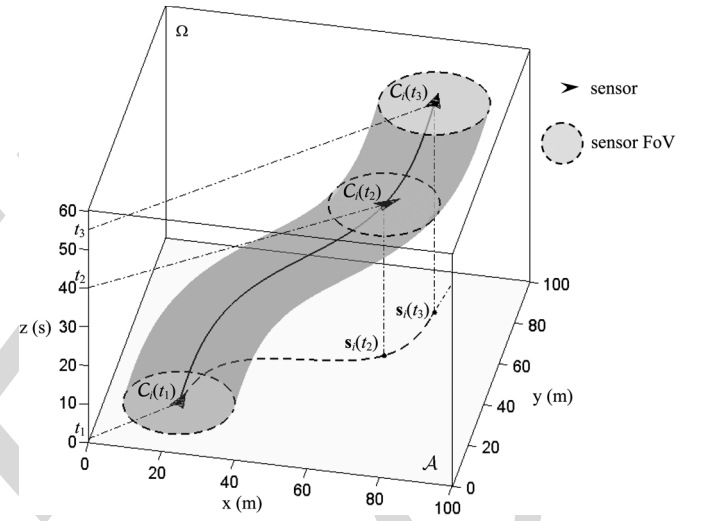


Fig. 2. Example of sensor trajectory and sensor FoV plotted at three moments in time  $t_1 = 1(s)$ ,  $t_2 = 40(s)$ , and  $t_3 = 55(s)$ .

129 detection as a function of the time-varying network state,  $\mathbf{s}(t)$ . Then,  
130 the detection probability function can be optimized subject to the  
131 network dynamic equation (1) using optimal control theory. From the  
132 detection model (3), the  $i$ th sensor has a nonzero probability to detect  
133 a target if and only if  $\|\mathbf{x}(t) - \mathbf{s}_i(t)\| \leq r_i$ . It can be shown that, as the  
134  $i$ th sensor moves along a trajectory  $\mathbf{s}_i(t)$ , the set of all tracks detected  
135 is contained by a time-varying three-dimensional coverage cone in  $\Omega$   
136 defined according to the following lemma:

**Lemma III.1:** The  $i$ th coverage cone defined as

$$K_i(t) = \{[xyz]^T \in \mathbb{R}^3 \mid t_j < z \leq t_{j+1},$$

$$\left\| [x \ y]^T - \frac{(z - t_j)}{(t - t_j)} [\mathbf{s}_i(t) - \mathbf{x}_j] - \mathbf{x}_j \right\| \leq \frac{(z - t_j)}{(t - t_j)} r_i \} \quad (6)$$

137 contains the set of all target tracks that intersect the  $i$ th sensor FoV,  
138  $C_i(t)$ , at any time  $t \in (t_j, t_{j+1}]$ .

**Proof:** Let the directed line segment  $\mathbf{m}_j(t) \subset \Omega$  represent a  
140 target track as it evolves from time  $t_j$  to  $t$ , such that

$$\mathbf{m}_j(t) = \left\{ \mathbf{y} \in \mathbb{R}^3 \mid \mathbf{y} = \mathbf{z}_j + \alpha \begin{pmatrix} \mathbf{x}^T(t) \\ t \end{pmatrix} - \mathbf{z}_j, \alpha \in (0, 1] \right\} \quad (7)$$

142 where  $\mathbf{z}_j = [\mathbf{x}_j^T \ t_j]^T$  is the segment origin in an inertial frame  $\mathcal{F}_\Omega$   
143 embedded in  $\Omega$ . Then, any point  $\mathbf{a} \in \mathbf{m}_j(t)$ , represented as a con-  
144 stant three-dimensional vector  $\mathbf{a} = [a_x \ a_y \ a_z]^T$ , obeys the equality,

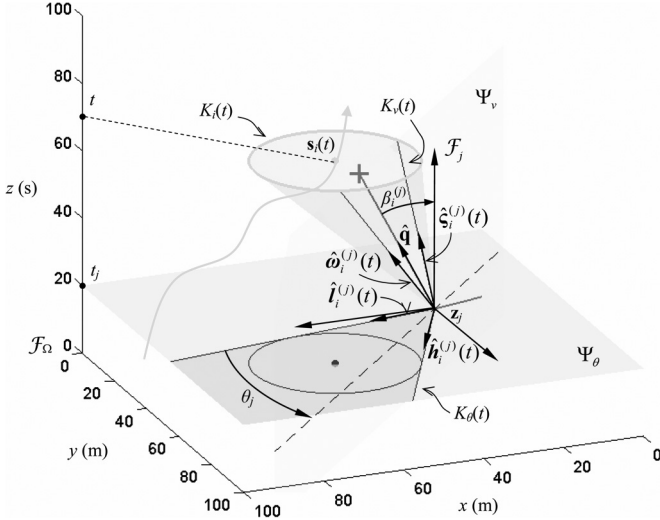


Fig. 3. Time-varying coverage cone (green) with its heading-cone (cyan) and velocity-cone (yellow) representations (adapted from [6]).

145  $[a_x \ a_y]^T = (a_z - t_j)[\mathbf{x}(t) - \mathbf{x}_j]/(t - t_j) + \mathbf{x}_j$ . From (3), a target at  
146  $\mathbf{a}$  is detected if and only if

$$\left\| [a_x \ a_y]^T - \frac{(a_z - t_j)}{(t - t_j)} [\mathbf{s}_i(t) - \mathbf{x}_j] - \mathbf{x}_j \right\| \leq \frac{(a_z - t_j)}{(t - t_j)} r_i. \quad (8)$$

147 Thus, from (6), any point on  $\mathbf{m}_j(t)$  contained by  $\mathcal{C}_i(t)$  must be  
148 contained by the coverage cone, and thus  $\mathbf{m}_j(t) \in K_i(t)$ . ■

149 As illustrated in Fig. 3, the above lemma extends the definition of  
150 the *fixed* spatio-temporal coverage cone presented in [6] to a *time-*  
151 *varying* coverage cone  $K_i(t)$  that is a function of the sensor trajectory  
152  $\mathbf{s}_i(t)$ . Because  $K_i(t)$  is a circular cone that is possibly oblique, a  
153 Lebesgue measure of the tracks contained by  $K_i(t)$  can be obtained  
154 by considering the pair of two-dimensional (2-D) cones, referred to as  
155 *heading cone* and *velocity cone* [6], and reviewed in the next section.

#### 156 A. Heading and Velocity Cones Representation

157 The heading cone, denoted by  $K_\theta(t)$ , contains all target headings  
158 that lead to a detection by the  $i$ th sensor at any time  $t \in (t_j, t_{j+1}]$  and,  
159 thus, it is obtained from the projection of  $K_i(t)$  onto the heading plane

$$\Psi_\theta \triangleq \{[x \ y \ z]^T \in \Omega \mid z = t_j\}. \quad (9)$$

160 Because  $K_\theta$  is a 2-D cone, it can be expressed as a linear combination  
161 of two unit vectors in  $\Psi_\theta$

$$\begin{aligned} \hat{\mathbf{h}}_{ij}(t) &= \begin{bmatrix} \cos \alpha_{ij}(t) & -\sin \alpha_{ij}(t) \\ \sin \alpha_{ij}(t) & \cos \alpha_{ij}(t) \\ 0 & 0 \end{bmatrix} \hat{\mathbf{d}}_{ij}(t) \triangleq \begin{bmatrix} \cos \phi_{ij}(t) \\ \sin \phi_{ij}(t) \\ 0 \end{bmatrix} \\ \hat{\mathbf{l}}_{ij}(t) &= \begin{bmatrix} \cos \alpha_{ij}(t) & \sin \alpha_{ij}(t) \\ -\sin \alpha_{ij}(t) & \cos \alpha_{ij}(t) \\ 0 & 0 \end{bmatrix} \hat{\mathbf{d}}_{ij}(t) \triangleq \begin{bmatrix} \cos \psi_{ij}(t) \\ \sin \psi_{ij}(t) \\ 0 \end{bmatrix} \end{aligned}$$

162 where

$$\begin{aligned} \hat{\mathbf{d}}_{ij}(t) &= [\mathbf{s}_i(t) - \mathbf{x}_j] / \|\mathbf{s}_i(t) - \mathbf{x}_j\| \\ \alpha_{ij}(t) &= \sin^{-1}(r_i / \|\mathbf{s}_i(t) - \mathbf{x}_j\|) \end{aligned}$$

163 such that the heading cone defined with respect to a local coordinate  
164 frame  $\mathcal{F}_j$  is

$$K_\theta[\mathbf{s}_i(t), \mathbf{z}_j] \triangleq \{c_1 \hat{\mathbf{h}}_{ij}(t) + c_2 \hat{\mathbf{l}}_{ij}(t) \mid c_1, c_2 \geq 0\}. \quad (10)$$

Examples of heading cone and heading plane are illustrated in Fig. 3, 165  
along with the unit vector representation. 166

The velocity cone, denoted by  $K_v(t)$ , contains all target speeds that 167  
lead to a detection by the  $i$ th sensor at any time  $t \in (t_j, t_{j+1}]$  and, thus, 168  
it is obtained from the intersection of  $K_i(t)$  with the velocity plane 169

$$\Psi_v \triangleq \left\{ \begin{bmatrix} x \\ y \\ z \end{bmatrix} \in \Omega \mid \begin{bmatrix} \sin \theta_j \\ \cos \theta_j \end{bmatrix}^T \begin{bmatrix} x \\ -y \end{bmatrix} = \begin{bmatrix} \sin \theta_j \\ \cos \theta_j \end{bmatrix} \mathbf{x}_j, z \geq t_j \right\}. \quad (11)$$

Similarly to the heading cone,  $K_v$  can be represented by two unit 170  
vectors 171

$$\begin{aligned} \hat{\mathbf{s}}_{ij}(t) &= [\sin \eta_{ij}(t) \cos \theta_j \quad \sin \eta_{ij}(t) \sin \theta_j \quad \cos \eta_{ij}(t)]^T \\ \hat{\mathbf{w}}_{ij}(t) &= [\sin \mu_{ij}(t) \cos \theta_j \quad \sin \mu_{ij}(t) \sin \theta_j \quad \cos \mu_{ij}(t)]^T \end{aligned}$$

where 172

$$\begin{aligned} \eta_{ij}(t), \mu_{ij}(t) &= \tan^{-1} \left[ \frac{1}{t - t_j} ([\cos \theta_j \sin \theta_j](\mathbf{s}_i(t) - \mathbf{x}_j) \right. \\ &\quad \left. \mp \sqrt{r_i^2 - ([\sin \theta_j - \cos \theta_j](\mathbf{s}_i(t) - \mathbf{x}_j))^2} \right) \end{aligned}$$

such that the velocity cone in  $\mathcal{F}_j$  is 173

$$K_v[\mathbf{s}_i(t), \mathbf{z}_j] \triangleq \{c_1 \hat{\mathbf{s}}_{ij}(t) + c_2 \hat{\mathbf{w}}_{ij}(t) \mid c_1, c_2 \geq 0\}. \quad (12)$$

Then, the pair of cones  $\{K_\theta(t), K_v(t)\}$ , defined in (10) and (12), 174  
can be used to represent all tracks in  $K_i(t)$ , as summarized by the 175  
following lemma (adapted from [6]). 176

**Lemma III.2:** A target track  $\mathbf{m}_j(t)$  is contained by the coverage 177  
cone  $K_i(t)$  if and only if its projection in  $\Psi_\theta$  is contained by the 178  
heading cone  $K_\theta(t)$ , and its projection in  $\Psi_v$  is contained by the 179  
corresponding velocity cone  $K_v(t)$ . 180

The proof of Lemma III.2 is a simple extension of the proof in [6]. 181

#### 182 B. SNMP Objective Function

The extremals of the heading and velocity cones presented in the 183  
previous section determine upper and lower bounds for the target 184  
heading angle and speed, respectively, that lead to a detection by 185  
the  $i$ th sensor, as functions of the time-varying sensor position  $\mathbf{s}_i$ . 186  
Let the intervals  $\mathcal{H}_{ij}(t) \triangleq [\psi_{ij}(t), \phi_{ij}(t)]$  and  $\mathcal{V}_{ij}(t) \triangleq [\tan \eta_{ij}(t),$  187  
 $\tan \mu_{ij}(t)]$  respectively denote the headings and speeds contained by 188  
the heading and velocity cones. Then, the probability that the  $i$ th sensor 189  
detects the target at any time  $t \in (t_j, t_{j+1}]$  is the probability that the 190  
Markov parameters are contained by the coverage cone  $K_i(t)$  191

$$P_d(i, j, t) = \int_{\mathcal{A} \times \mathcal{H}_{ij}(t) \times \mathcal{V}_{ij}(t)} f_{\mathbf{x}_j, \Theta_j, V_j}(\mathbf{x}_j, \theta_j, v_j) d\mathbf{x}_j d\theta_j dv_j \quad (13)$$

where  $f_{\mathbf{x}_j, \Theta_j, V_j}(\cdot)$  is the joint pdf of the Markov parameters  $\mathbf{x}_j$ ,  $\theta_j$ , 192  
and  $v_j$ . Since these parameters are independent random variables, the 193  
probability of detection can be simplified to 194

$$\begin{aligned} P_d(i, j, t) &= \int_{\mathcal{A} \times \mathcal{H}_{ij}(t) \times \mathcal{V}_{ij}(t)} f_{\mathbf{x}_j}(\mathbf{x}_j) f_{\Theta_j}(\theta_j) f_{V_j}(v_j) d\mathbf{x}_j d\theta_j dv_j \\ &= \int_{\mathbf{x}_j \in \mathcal{A}} f_{\mathbf{x}_j}(\mathbf{x}_j) \int_{\psi_{ij}(t)}^{\phi_{ij}(t)} f_{\Theta_j}(\theta_j) \int_{\tan \eta_{ij}(t)}^{\tan \mu_{ij}(t)} f_{V_j}(v_j) dv_j d\theta_j d\mathbf{x}_j \\ &\quad \forall t \in (t_j, t_{j+1}]. \end{aligned} \quad (14)$$

It can be seen that using the 2-D coverage cones reduces the region of integration from  $\Omega$  to the product space  $\mathcal{A} \times \mathcal{H}_{ij}(t) \times \mathcal{V}_{ij}(t)$ , and thus reduces the computation required to evaluate the detection probability. Then, the objective function for the SNMP problem can be obtained by integrating over time the probability of independent sensor detections by the  $n$  sensors for all  $m$  time intervals, as follows:

$$\begin{aligned} J &= -\frac{1}{n} \sum_{i=1}^n \sum_{j=1}^m \int_{t_j}^{t_{j+1}} P_d(i, j, t) dt \\ &= -\frac{1}{n} \sum_{i=1}^n \sum_{j=1}^m \int_{t_j}^{t_{j+1}} \int_{\mathcal{A}} f_{\mathbf{x}_j}(\mathbf{x}_j) \int_{\psi_{ij}(t)}^{\phi_{ij}} (t) f_{\Theta_j}(\theta_j) \\ &\quad \times \int_{\tan \mu_{ij}(t)}^{\tan \nu_{ij}(t)} f_{V_j}(v_j) dv_j d\theta_j d\mathbf{x}_j dt. \end{aligned} \quad (15)$$

The above objective function is to be optimized subject to the network dynamics (1) and the inequality constraints on the network state and control given by  $\mathbf{c}[\mathbf{s}(t)] \leq \mathbf{0}_{(n-1)n \times 1}$  and (2), respectively. The inequality constraint on the state is defined as the vector function  $\mathbf{c} = [c_{12} \cdots c_{il} \cdots c_{n(n-1)}]^T$ , where

$$c_{il} \triangleq (r_i + r_l)^2 - \|\mathbf{s}_i(t) - \mathbf{s}_l(t)\|^2, \quad i, l = 1, \dots, n, \quad i \neq l$$

and is used to guarantee independent sensor detections (see [5] and references therein for a comprehensive treatment of detection theory). Therefore, the SNMP problem can be formulated as the following optimal control problem:

$$\begin{aligned} \min \quad & J \\ \text{sbj. to} \quad & \dot{\mathbf{s}}(t) = \mathbf{A}\mathbf{s}(t) + \mathbf{B}\mathbf{u}(t) \\ & \mathbf{c}[\mathbf{s}(t)] \leq \mathbf{0} \\ & -\mathbf{1} \leq \mathbf{u}(t) \leq \mathbf{1}. \end{aligned} \quad (16)$$

Because  $J$  is not quadratic, the above SNMP optimal control problem must be solved numerically for the optimal state and control trajectories  $\mathbf{s}^*(t)$  and  $\mathbf{u}^*(t)$ . Section IV derives the SNMP EL equations, and explains how their numerical solution can be obtained via VIM. The VIM numerical simulation results and complexity analysis are presented in Section V.

#### IV. OPTIMAL CONTROL SOLUTION

In order to maximize the detection probability and minimize the control usage, the SNMP objective function is chosen to be of the Lagrange type, with Lagrangian

$$\begin{aligned} \mathcal{L}[\mathbf{s}(t), \mathbf{u}(t), t] &= -\sum_{i=1}^n \sum_{j=1}^m \int_{\mathcal{A}} f_{\mathbf{x}_j}(\mathbf{x}_j) \int_{\psi_{ij}(t)}^{\phi_{ij}} (t) f_{\Theta_j}(\theta_j) \\ &\quad \times \int_{\tan \mu_{ij}(t)}^{\tan \nu_{ij}(t)} f_{V_j}(v_j) dv_j d\theta_j d\mathbf{x}_j + \alpha \mathbf{u}^T \mathbf{u}. \end{aligned} \quad (17)$$

To find the necessary conditions for optimality, the Hamiltonian

$$\begin{aligned} \mathcal{H} &\triangleq \mathcal{L}[\cdot] + \lambda^T(t) [\mathbf{A}\mathbf{s}(t) + \mathbf{B}\mathbf{u}(t)] + \gamma^T(t) \mathbf{c}[\mathbf{s}(t)] \\ &= \mathcal{H}[\mathbf{s}(t), \mathbf{u}(t), \lambda(t), \gamma(t)] \end{aligned} \quad (18)$$

is introduced, adjoining the constraints on the state and control to (17) by means of the Lagrange multipliers  $\lambda$  and  $\gamma$ .

Then, the SNMP Euler–Lagrange equations are

$$\dot{\lambda}(t) = -(\partial \mathcal{L}[\cdot] / \partial \mathbf{s})^T - \mathbf{A}^T \lambda(t) - (\partial \mathbf{c}[\cdot] / \partial \mathbf{s})^T \gamma(t) \quad (19)$$

$$\lambda(T_f) = \mathbf{0} \quad (20)$$

$$(\partial \mathcal{L}[\cdot] / \partial \mathbf{u})^T + \mathbf{B}^T \lambda(t) + (\partial \mathbf{c}[\cdot] / \partial \mathbf{u})^T \gamma(t) = \mathbf{0} \quad (21)$$

where  $\partial \mathcal{L} / \partial \mathbf{s} = [(\partial \mathcal{L} / \partial \mathbf{s}_1)^T \cdots (\partial \mathcal{L} / \partial \mathbf{s}_n)^T]^T$ . Letting  $\xi_{ij}$ ,  $\zeta_{ij} = (\psi_{ij} \mp \phi_{ij})/2$ , the partial derivatives of the Lagrangian with respect to the state can be approximated as

$$\frac{\partial \mathcal{L}}{\partial \mathbf{s}_i} \approx \left[ \rho \int_{\mathcal{A}} \{ f_{\mathbf{x}_j}(\mathbf{x}_j) \xi_{ij}(\mathbf{s}_i, \mathbf{x}_j) \sin[\zeta_{ij}(\mathbf{s}_i, \mathbf{x}_j)] \} d\mathbf{x}_j \right. \\ \left. \rho \int_{\mathcal{A}} \{ f_{\mathbf{x}_j}(\mathbf{x}_j) \xi_{ij}(\mathbf{s}_i, \mathbf{x}_j) \cos[\zeta_{ij}(\mathbf{s}_i, \mathbf{x}_j)] \} d\mathbf{x}_j \right] \triangleq \mathbf{g}_i[\mathbf{s}_i(t)] \quad (22)$$

where  $\rho = -8 \ln(\pi/2) / (|V_j| |\Theta_j| (t - t_j))$  and  $|\cdot|$  denotes the variable's range, and the partial derivative of the Lagrangian with respect to the control is  $\partial \mathcal{L} / \partial \mathbf{u} = \alpha \mathbf{u}^T(t)$ . Since  $\partial \mathbf{c} / \partial \mathbf{u} = \mathbf{0}$ , (21) simplifies to  $\alpha \mathbf{u}(t) + \mathbf{B}^T \lambda = \mathbf{0}$  and, thus

$$\mathbf{u}(t) = -\frac{1}{\alpha} \mathbf{B}^T \lambda(t). \quad (23)$$

Now, from the transition matrix solution of the state-space form (1),  $\mathbf{s}(t) = e^{\mathbf{A}(t-T_0)} \mathbf{s}_0 + \int_{T_0}^t \mathbf{B} \mathbf{u}(\tau) d\tau$ , and, thus, from (23) it follows that

$$\mathbf{s}(t) = e^{\mathbf{A}(t-T_0)} \mathbf{s}_0 - \frac{1}{\alpha} \int_{T_0}^t \mathbf{B} \mathbf{B}^T \lambda(\tau) d\tau. \quad (24)$$

Because  $\gamma = \mathbf{0}$  when  $\mathbf{c}[\mathbf{s}(t)] \neq \mathbf{0}$ , it also follows from (24) that the first optimality condition (19) can be simplified to

$$\dot{\lambda}(t) = -\mathbf{g}[\mathbf{s}(t)] \left( \int_0^t \mathbf{B} \mathbf{B}^T \lambda(\tau) d\tau \right) - \mathbf{A}^T \lambda(t) \quad (25)$$

where the vector function  $\mathbf{g}[\cdot] \triangleq [\mathbf{g}_1^T[\cdot] \cdots \mathbf{g}_n^T[\cdot]]$  is defined according to (22). Thus, (25) represents a set of integro-differential equations with boundary conditions (20).

Many algorithms have been developed for solving integro-differential equations, including the Adomian decomposition method [18], the homotopy perturbation method [19], and the VIM [20]. In this technical note, VIM is chosen to solve (25) because its intermediate approximations are known to converge rapidly to an accurate solution. VIM starts with a linear trial function and obtains higher order terms iteratively as follows:

$$\begin{aligned} \lambda^{(\ell+1)}(t) &= \lambda^{(\ell)}(t) \\ &\quad - \int_{T_0}^t \left\{ \mathbf{A}^T \lambda^{(\ell)}(\sigma) - \mathbf{g}[\mathbf{s}(t)] \left[ \int_{T_0}^{\sigma} \mathbf{B} \mathbf{B}^T \lambda^{(\ell)}(\tau) d\tau \right] \right\} d\sigma \end{aligned} \quad (26)$$

where the superscript  $\ell$  denotes the  $\ell$ th-order approximation.

By exploiting the integro-differential structure of the EL equations, VIM can significantly reduce computational complexity when compared to direct methods of solution. In direct methods, the dynamic equation and objective function are discretized and transcribed into an NLP that, typically, is solved using sequential quadratic programming (SQP) [21]. The computational complexity of SQP direct methods is  $O(n^3 K^3 M)$ , where  $n$  is the number of sensors,  $K$  is the number of

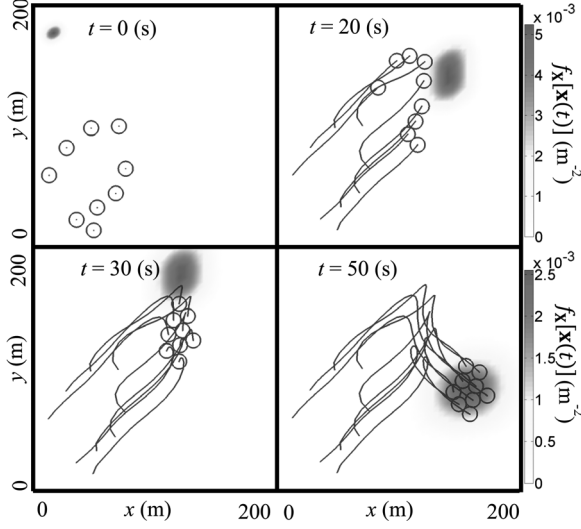


Fig. 4. Optimal sensor trajectories for  $n = 9$  and  $r_i = 6$  (m), given the target motion model in Table I.

254 collocation points, and  $M$  is the number of iterations required for  
 255 convergence [21]. The indirect VIM, on the other hand, requires a  
 256 computation time of  $O(nK^2)$  to evaluate (26) using Euler integration.  
 257 Therefore, the computation complexity for VIM is  $O(nK^2M)$ , where  
 258 in practice  $M$  is quite small. Therefore, the VIM solution is efficient  
 259 for mobile sensor networks with a few dozen sensors. For larger  $n$ ,  
 260 efficient solutions can be obtained by combining the results in this  
 261 technical note with the distributed optimal control approach presented  
 262 in [22].

## V. SIMULATION RESULTS

264 Consider the Markov motion model in Table I for a target traversing  
 265 the RoI over a time interval  $(T_0, T_f] = (0, 50](s)$ , where  $m = 5$ . At  
 266  $t_1 = T_0 = 0$  (s), the pdf of the target position,  $f_{\mathbf{x}_1}(\mathbf{x}_1)$ , is a 2-D mul-  
 267 tivariate Gaussian distribution, denoted by  $\mathcal{N}(\boldsymbol{\mu}, \boldsymbol{\Sigma})$ , with mean  $\boldsymbol{\mu} =$   
 268  $[20 \ 180]^T$  (m) and covariance matrix  $\boldsymbol{\Sigma} = \text{diag}([10 \ 10])$  (m<sup>2</sup>),  
 269 where,  $\text{diag}(\cdot)$  denotes an operator that places a row vector on the  
 270 diagonal of a zero matrix. The heading and velocity pdfs are uniform  
 271 distributions, denoted by  $\mathcal{U}(a, b)$ , with support  $[a, b]$ , as shown in  
 272 Table I. Then, the pdfs of  $\mathbf{x}_2, \dots, \mathbf{x}_5$ , can be computed recursively,  
 273 as shown in [6].

274 Simulation results are presented for two example cases, one network  
 275 with  $n = 9$  and  $r_i = 6$  (m) (Fig. 4), and one network with  $n = 20$   
 276 and  $r_i = 5$  (m) (Fig. 5). Figs. 4 and 5 show the sensor trajectories and  
 277 FoVs, and the pdf of the target position, at four sample instants in time.  
 278 It can be seen that by the geometric transversals approach the sensors  
 279 plan their motion such that the detection probability in  $(T_0, T_f]$  is  
 280 maximized. The optimal control histories of a randomly chosen sensor  
 281 (red arrow in Fig. 5) are plotted in Fig. 6 to illustrate that control  
 282 inputs obtained by this approach are smooth and obey the desired  
 283 bounds in (2).

284 The effectiveness of the geometric transversals approach is illus-  
 285 trated by comparing the probability of detection obtained by the  
 286 network in Fig. 5 to that obtained by potential field, greedy, uniform  
 287 grid, and random algorithms. In potential field [23], the pdf of the  
 288 target position is used to build an attractive potential, and a repulsive  
 289 force  $f_r = -c_r / \|\mathbf{s}_i(t) - \mathbf{s}_j(t)\|^2$  is used to prevent collisions between  
 290 sensors, where  $c_r = 1$  [23]. The greedy algorithm proposed in [24]  
 291 places the sensors at  $n$  fixed locations, such that the network cover-  
 292 age is maximized while retaining line-of-sight relationships between

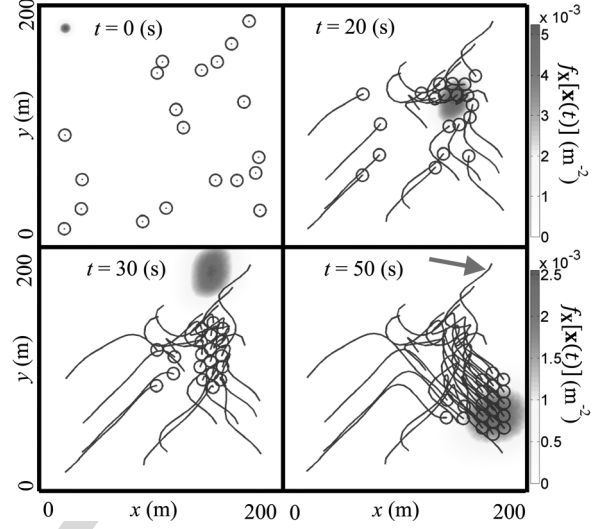


Fig. 5. Optimal sensor trajectories for  $n = 20$  and  $r_i = 5$  (m), given the target motion model in Table I.

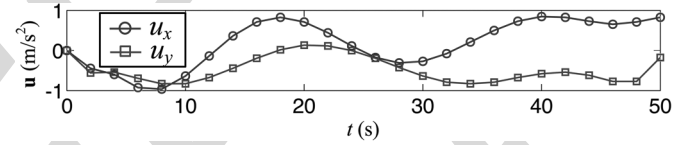


Fig. 6. Optimal control histories of one sensor chosen at random from the network in Fig. 5 (as shown by red arrow).

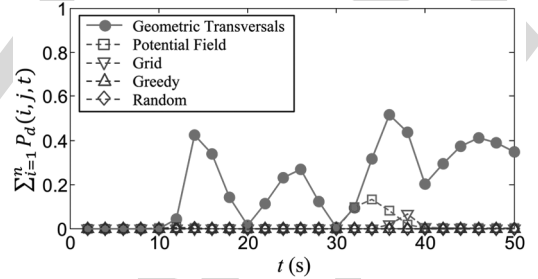


Fig. 7. Performance comparison for sensor network in Fig. 5, with  $n = 20$ ,  $r_i = 5$  (m), and the target motion model in Table I.

293 sensors. The grid and random algorithms proposed in [25] place the  
 294 sensors at  $n$  fixed locations in  $\mathcal{A}$  according to a uniformly spaced grid  
 295 or by sampling a uniform distribution.

296 The results in Fig. 7 are representative of extensive simulations  
 297 performed using different sensor networks, target models, and initial  
 298 conditions. Because the network performance is highly sensitive to  
 299 initial conditions, the average probability of detection, denoted by  $P_e$ ,  
 300 is computed by considering over 100 initial conditions, sampled uni-  
 301 formly at random from the RoI, holding network and target parameters  
 302 constant. The mean performance ( $P_e$ ) and three standard deviations  
 303 (SDs) obtained by the five algorithms are plotted in Fig. 8 and show  
 304 that the geometric transversals approach significantly outperforms  
 305 other algorithms over the entire time interval  $(T_0, T_f]$ .

## VI. SUMMARY AND CONCLUSIONS

306 This technical note presents a geometric transversals approach for  
 307 planning the motion of a mobile sensor network such that its detection  
 308 probability is maximized over time. By this approach, the approach  
 309 derives a track coverage objective function in closed form, based on  
 310



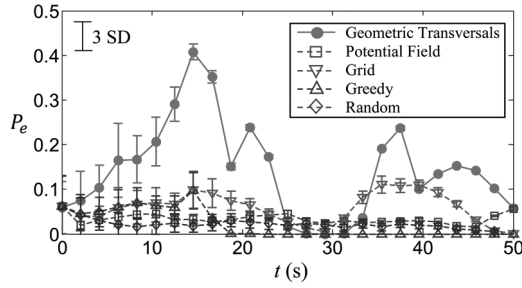


Fig. 8. Probability of detection averaged over 100 initial conditions for  $n = 20$ ,  $r_s = 5$  (m), and the target motion model in Table I.

the transition pdfs of the target Markov motion model. By this novel approach, the probability of detection can be optimized subject to the sensor kinodynamic equations, and inequality constraints on the sensor state and control. The necessary conditions for optimality are derived and reduced to a set of integro-differential equations that are solved numerically using a variational iteration method. The results show that by this approach the computational complexity is significantly reduced compared to a direct method, and the detection probability is significantly increased compared to existing potential field, greedy, grid, or random algorithms.

#### REFERENCES

- [1] I. F. Akyildiz, W. Su, Y. Sankarasubramaniam, and E. Cayirci, "Wireless sensor networks: A survey," *Comput. Netw.*, vol. 38, no. 4, pp. 393–422, 2002.
- [2] D. Chen and P. K. Varshney, "Qos support in wireless sensor networks: A survey," in *Proc. Int. Wireless Netw. Conf.*, 2004, vol. 233.
- [3] X. R. Li and V. P. Jilkov, "Survey of maneuvering target tracking. part i. dynamic models," *IEEE Trans. Aerosp. Electron. Syst.*, vol. 39, no. 4, pp. 1333–1364, 2003.
- [4] K. Baumgartner and S. Ferrari, "A geometric transversal approach to analyzing track coverage in sensor networks," *IEEE Trans. Comput.*, vol. 57, no. 8, pp. 1113–1128, Aug. 2008.
- [5] T. A. Wettergren, "Performance of search via track-before-detect for distributed sensor networks," *IEEE Trans. Aerosp. Electron. Syst.*, vol. 44, no. 1, pp. 314–325, Jan. 2008.
- [6] H. Wei and S. Ferrari, "A geometric transversals approach to analyzing the probability of track detection for maneuvering targets," *IEEE Trans. Comput.*, vol. 63, no. 11, pp. 2633–2646, Nov. 2013.
- [7] Y. Bar-Shalom and X. R. Li, *Multitarget-Multisensor Tracking: Principles and Techniques*. Storrs, CT, USA: Yaakov Bar-Shalom, 1995.
- [8] P. Fiorini and Z. Shiller, "Motion planning in dynamic environments using velocity obstacles," *Int. J. Robot. Res.*, vol. 17, no. 7, pp. 760–772, 1998.
- [9] H. Wei, W. Lu, P. Zhu, G. Huang, J. Leonard, and S. Ferrari, "Optimized visibility motion planning for target tracking and localization," in *Proc. IEEE/RSJ Int. Conf. Intell. Robots Syst. (IROS 2014)*, 2014, pp. 76–82.
- [10] J. Betts, "Survey of numerical methods for trajectory optimization," *J. Guid., Control, Dynam.*, vol. 21, no. 2, pp. 193–207, 1998.
- [11] Y. Bar-Shalom and X.-R. Li, *Estimation and Tracking: Principles, Techniques, Software*, vol. 393. Norwood, MA, USA: Artech House, 1993.
- [12] H. Wei, W. Ross, S. Varisco, P. Krief, and S. Ferrari, "Modeling of human driver behavior via receding horizon and artificial neural network controllers," in *Proc. IEEE Ann. Conf. Decision Control (CDC)*, Florence, Italy, Dec. 2013, pp. 6778–6785.
- [13] B. Liu and D. Towsley, "A study of the coverage of large-scale sensor networks," in *Proc. IEEE Int. Mobile Ad-hoc Sensor Syst. Conf.*, 2004, pp. 475–483.
- [14] H. Wei, W. Lu, and S. Ferrari, "An information value function for nonparametric gaussian processes," in *Proc. Neural Inform. Process. Syst. Conf.*, Lake Tahoe, NV, USA, 2012.
- [15] J. Yick, B. Mukherjee, and D. Ghosal, "Wireless sensor network survey," *Comput. Netw.*, vol. 52, no. 12, pp. 2292–2330, 2008.
- [16] H. Wei, W. Lu, P. Zhu, S. Ferrari, R. H. Klein, S. Omidshafiei, and J. P. How, "Camera control for learning nonlinear target dynamics via bayesian nonparametric dirichlet-process gaussian-process (DP-GP) models," in *Proc. IEEE/RSJ Int. Intell. Robots Syst. Conf. (IROS 2014)*, pp. 95–102.
- [17] S. Meyn and R. L. Tweedie, *Markov Chains and Stochastic Stability*, 2nd ed. New York, NY, USA: Cambridge Univ. Press, 2009, ser. Cambridge Mathematical Library.
- [18] G. Adomian, "A review of the decomposition method and some recent results for nonlinear equations," *Mathemat. Comput. Modell.*, vol. 13, no. 7, pp. 17–43, 1990.
- [19] J.-H. He, "Homotopy perturbation technique," *Comput. Methods Appl. Mech. Eng.*, vol. 178, no. 3, pp. 257–262, 1999.
- [20] B. Neta, "Numerical solution of a nonlinear integro-differential equation," *J. Mathemat. Anal. Appl.*, vol. 89, no. 2, pp. 598–611, 1982.
- [21] M. J. D. Powell, "A fast algorithm for nonlinearly constrained optimization calculations," *Numer. Anal.*, vol. 630, 1978.
- [22] G. Foderaro, S. Ferrari, and T. Wettergren, "Distributed optimal control for multi-agent trajectory optimization," *Automatica*, vol. 50, pp. 149–154, 2014.
- [23] S. S. Ge and Y. J. Cui, "Dynamic motion planning for mobile robots using potential field method," *Auton. Robots*, vol. 13, no. 3, pp. 207–222, 2002.
- [24] A. Howard, M. J. Matarí, and G. S. Sukhatme, "An incremental self-deployment algorithm for mobile sensor networks," *Auton. Robots*, vol. 13, pp. 113–126, 2002.
- [25] H. Gonzales-Banos and J. C. Latombe, "Robot motion planning with uncertainty in control and sensing," in *Proc. 17th Ann. Symp. Computational Geom. (SCG'01)*, Boston, MA, USA, 2001.

## AUTHOR QUERY

NO QUERY.

IEEE  
Proof